Unifying deterministic and stochastic ecological dynamics via a landscape-flux approach

Li Xu[a], Denis Patterson[b,c], Ann Carla Staver[d], Simon Asher Levin[e,1], and Jin Wang[f,1]

[a]State Key Laboratory of Electroanalytical Chemistry, Changchun Institute of Applied Chemistry, Chinese Academy of Sciences, Changchun 130022, People's Republic of China; [b]High Meadows Environmental Institute, Princeton University, Princeton, NJ 08544; [c]Department of Mathematics, Brandeis University, Waltham, MA 02454; [d]Department of Ecology and Evolutionary Biology, Yale University, New Haven, CT 06520; [e]Department of Ecology and Evolutionary Biology, Princeton University, Princeton, NJ 08544; and [f]Department of Chemistry, Physics and Applied Mathematics, State University of New York at Stony Brook, Stony Brook, NY 11794-3400

Contributed by Simon Asher Levin, April 23, 2021 (sent for review March 1, 2021; reviewed by Jie Liang and Qing Nie)

The frequency distributions can characterize the population-potential landscape related to the stability of ecological states. We illustrate the practical utility of this approach by analyzing a forest–savanna model. Savanna and forest states coexist under certain conditions, consistent with past theoretical work and empirical observations. However, a grassland state, unseen in the corresponding deterministic model, emerges as an alternative quasi-stable state under fluctuations, providing a theoretical basis for the appearance of widespread grasslands in some empirical analyses. The ecological dynamics are determined by both the population-potential landscape gradient and the steady-state probability flux. The flux quantifies the net input/output to the ecological system and therefore the degree of nonequilibriumness. Landscape and flux together determine the transitions between stable states characterized by dominant paths and switching rates. The intrinsic potential landscape admits a Lyapunov function, which provides a quantitative measure of global stability. We find that the average flux, entropy production rate, and free energy have significant changes near bifurcations under both finite and zero fluctuation. These may provide both dynamical and thermodynamic origins of the bifurcations. We identified the variances in observed frequency time traces, fluctuations, and time irreversibility as kinematic measures for bifurcations. This framework opens the way to characterize ecological systems globally, to uncover how they change among states, and to quantify the emergence of quasi-stable states under stochastic fluctuations.

landscape | flux | global stability | ecological system

The characterization of the dynamics of systems through the construction of sets of differential equations and the exploration of their long-term behavior have become standard and powerful tools in the applied sciences (1). This is particularly the case in mathematical biology and ecology, from the early works of Volterra up to recent years (2). The framework of nonlinear dynamical systems allows us to efficiently characterize steady states, periodic orbits, and even more complex invariant sets, as well their dependence on system parameters (3–8). However, these methods often rely on local properties of the systems in the vicinity of attractors and are not designed to address how the dynamics are altered in the presence of noise or how fluctuations can induce global switching between multiple stable attractors. In many ecological models, multiple alternative stable states can emerge, each with their own distinct basin of attraction. Characterizing the stability of such states and their responses to ecological fluctuations and predicting the possible transitions among them is thus a grand challenge in ecology (3, 7, 9). Indeed, on longer time scales, slow variable evolution, perhaps initiated by fluctuations, can alter the topology of the dynamics, leading to critical transitions or to flickering between states or basins of attraction (1, 5, 6, 10–12). We present how landscape-flux theory from nonequilibrium statistical mechanics can provide a powerful framework to study these questions, using a well-known savanna–forest model, typically referred to as the Staver–Levin (SL) model, as a case study (5, 6). Here, savanna refers to a grass-dominated state with some trees and saplings while forest refers to a tree-dominated state with few grasses and saplings.

Ecological systems are subject to multifarious sources of stochastic noise, ranging from fires and climatic variability to variations in the growth and death rates of species (see refs. 5, 6, 8, 13, and 14 and the references therein). In ecological dynamics, the observables of interest fluctuate, which can introduce unpredictability into an otherwise deterministic process. In such settings, the statistics of vegetation or their distributions can be collected and often provide a reliable quantification of the state of an ecological system. The statistical patterns are typically relatively regular and the associated probabilistic dynamics can be predicted since they typically follow the linear evolution law dictated by the associated Fokker–Planck or Master equation. Although the probabilistic evolution equation and the corresponding Langevin equation for the stochastic trajectories are usually mathematically equivalent in terms of the statistics, the individual trajectories as a result of the nonlinear interactions and fluctuations are often impossible to reliably predict (1, 15, 16). These trajectories can be compared with observations

Significance

Characterizing stability and dynamics of ecological systems under fluctuations is a longstanding challenge in ecology. We study the ecodynamics of a forest–savanna model under fluctuations via a landscape-flux theoretical framework from nonequilibrium statistical physics and show that ecological dynamics are determined by both population landscape gradients and steady-state probability fluxes. Savanna and forest states coexist under certain conditions, and a grassland state unseen in deterministic cases emerges under fluctuations. The intrinsic landscape is identified with a Lyapunov function for quantifying global stability of ecological systems. We quantify barrier heights, kinetic paths, and switching rates between stable states. Average flux, entropy production rate, time irreversibility, variances in time traces, and fluctuations serve as markers to quantify onset/offset of bifurcations.

Author contributions: A.C.S., S.A.L., and J.W. designed research; L.X. performed research; A.C.S., S.A.L., and J.W. contributed new reagents/analytic tools; L.X., D.P., A.C.S., S.A.L., and J.W. analyzed data; and L.X., D.P., A.C.S., S.A.L., and J.W. wrote the paper.

Reviewers: J.L., University of Illinois at Chicago; and Q.N., University of California, Irvine.

The authors declare no competing interest.

[1]To whom correspondence may be addressed. Email: slevin@princeton.edu or jin.wang.1@stonybrook.edu.

This article contains supporting information online at https://www.pnas.org/lookup/suppl/doi:10.1073/pnas.2103779118/-/DCSupplemental.

Published June 11, 2021.

of not only the time traces, but also their frequency or statistical distributions, which are increasingly becoming available (17). A critical question is then how observed frequency distributions are linked to stability (18). Ecological analyses of snapshot data have mostly assumed that stable states will appear more frequently than unstable ones (19). However, the real situation can be more complicated, and it remains a challenge to disentangle the underlying stable configurations and stochastic effects.

Historically, researchers have applied a myriad of techniques to study the global dynamics of complex systems subject to random forcing. Some approaches have focused on the zero-noise limit (20–23) while others have considered the finite stochastic fluctuations (1, 24–26), but certain mathematical challenges still remain (25, 26). Data-driven approaches to landscape changes and transition paths have recently been explored in the microenvironment "ecosystem" of cancer–immune interactions (27–30). In this study, we highlight a recently developed method for analyzing the global stability and dynamics of both deterministic and stochastic complex systems in a unified framework (4, 17, 31, 32). For general dynamical systems, one can study the global dynamics by identifying the so-called population-potential landscape and the rotational curl flux. The global population-potential landscape is determined by the steady-state probability distribution of ecological states, while the rotational curl flux is determined by the steady-state probability flux. Heuristically, the population-potential landscape attracts the system to the basins of the steady states and the curl flux drives the system in a rotational way that reinforces the stability of the flow. Furthermore, since the population-potential landscape is directly associated with the statistical distribution of the steady states, we can use the observed frequency distribution to infer the underlying population-potential landscape. The observed frequency distributions are typically univariate, allowing an effective description of the ecological system in this specific dimension (8). The corresponding landscape inferred from the observed univariate frequency distribution can provide insights regarding the global stability of the system. If different univariate frequency distributions are observed, one may approximate the multivariate population landscape as the product of the individual univariate distributions (mean field approximation) under the weak coupling assumption. To obtain more precise information on the population landscape, one needs to know the time series of all of the observables for the joint distribution, which is rarely the case in practice.

Since the foundational work of Volterra (2), a significant amount of research has focused on trying to find Lyapunov functions for dynamic ecological models (33), but such approaches have practical difficulties and are still somewhat incomplete (4, 17, 31). The landscape-flux framework provides a general way to analyze the dynamics of ecological systems. We focus on its implications in a forest–savanna model to study the stochastic dynamics and the interplay between grass, saplings, and trees (5, 6). This will allow us to not only quantify the underlying population-potential landscape, link this to the frequency distribution of the observables at long times, and gain insights on the global stability under various conditions, but also characterize the effects of fluctuations on the dynamics.

This study establishes a link between the observed frequency distribution at long times and the population landscape of the ecological system. Moreover, we will identify the rates of transitions between multiple states and their dependence on noise levels. In particular, contrasting with the view that fluctuations destabilize steady states, we will show that here, fluctuations can sometimes produce a state not present in deterministic dynamics. Importantly, we show that the nonzero flux characterizing the net input/output to the ecological system and therefore the degree of nonequilibriumness (the distance away from equilibrium), together with the population-potential landscape, determine the noise-induced transitions between the basins of attraction, in terms of both the dominant paths and rates of transition. These noise-induced transitions are irreversible, in the sense that the dominant forward path from A to B is not the same as the dominant backward path from B to A. This framework thus opens the way to characterize the ecological system globally, to uncover how they switch between states due to the nonzero flux, and to quantify the emergence of stable states that are not present in the deterministic dynamics.

To study the SL model subject to noise, we first compute the nonequilibrium population-potential landscape (U) under finite fluctuations. We then take the zero-fluctuation limit to obtain the intrinsic potential landscape, denoted by ϕ_0. As we show presently, the intrinsic potential landscape is a global Lyapunov function for the ecological dynamics and thus the topological structure of the intrinsic potential landscape provides a quantitative measure for the global stability of the ecological system. In addition, we characterize the quantitative relationship between the driving force of the intrinsic potential gradient and that of the probabilistic flux for the ecological dynamics. We also identify the nonequilibrium free energy as a Lyapunov function for quantifying the global stability of the ecological systems at finite fluctuations. The linkage of the nonequilibrium intrinsic free energy with the different phases and the bifurcations (phase transitions) of the ecological system changes with respect to changes in the parameters.

Complex ecological systems often involve nonlinear interactions that can lead to a variety of behaviors and transitions between various dynamic regimes. These changes in the qualitative behavior of the system can be described by bifurcations where different stable/unstable states can branch out, meet, or emerge spontaneously (1, 34, 35). Energy, material, or information exchange can also lead to new phases and bifurcations. In nonequilibrium systems, the flux provides the origin of the entropy production, which is a measure of nonequilibrium thermodynamic cost. This cost is a thermodynamic measure of the free-energy consumption or dissipation needed for certain biological functions; it is quantified by the entropy production. For example, to maintain the cell cycle flow, nutrition supply through the phosphorylation reaction via adenosine triphosphate hydrolysis, quantified by the entropy production or free-energy cost, is required. In an equilibrium ecological system, the bifurcations are determined exclusively by the potential gradient. However, in nonequilibrium ecological systems, the bifurcations are determined by both the potential gradient and the rotational flux. Therefore, the curl flux plays a crucial role in the emergence of nonequilibrium states and bifurcations in nonequilibrium systems (4, 36, 37).

We analyze the average curl flux, Flux_{av}, and entropy production rate, EPR, under both finite and zero fluctuations. As system parameters vary, Flux_{av} and the associated thermodynamic cost in terms of the EPR both have significant changes near (between) the two saddle-node bifurcations, especially in the zero-fluctuation case. Therefore, the dynamical and thermodynamic origins of the bifurcation for nonequilibrium ecological systems may be from the curl flux and the EPR, respectively. On the other hand, these physical quantities can be inferred from the observed time series. For example, information on flux and EPR can be inferred directly from the time irreversibility of the observed time traces. The variance in the frequency statistics and kinetic time obtained directly from the observed time traces can be used as the kinematic markers for the onset or offset of bifurcations. Both physical and kinematic markers based on the observed time traces may be used to identify the start or end of bifurcations in ecological dynamics.

Materials and Methods

The Staver–Levin Model. The SL model was introduced to study the dynamics of the ecological system and the interplay between the fractions of terrain covered by grass (G), savanna saplings (S), and savanna trees (T) in a forest–savanna ecological system (5, 6). In the absence of forest trees, the interaction between savannas and grass is mediated by fires, carried by grass, that limit the rate of maturation of savanna saplings into adult trees. More precisely, the simplified interactions between grass and two life stages of savanna trees are given by the equations (5, 6)

$$\begin{aligned}\dot{G} &= \mu S + \nu T - \beta G T\\ \dot{S} &= \beta G T - (\omega(G) + \mu) S\\ \dot{T} &= \omega(G) S - \nu T.\end{aligned} \quad [1]$$

Parameter interpretations and their default values (unless otherwise specified) are given in Table 1. The function $\omega(G) = \omega_0 + \frac{\omega_1 - \omega_0}{1+e^{-(G-\theta_1)/ss_1}}$ is a smooth decreasing sigmoid with parameters chosen to qualitatively capture how threshold fire onset limits the maturation of saplings into adult trees. This aspect of the model can be motivated by percolation theory as well as empirical observations (6, 38). By scanning the parameter ranges, we find only monostable or bistable behaviors (see *SI Appendix* for detailed exploration of the parameter space). Therefore, we focus on certain ranges of parameters, which cover all of the dynamic regimes of the model.

The SL model assumes that all terrain is covered by one of grass, saplings, or savanna trees, so that $G + S + T = 1$ for all times. Hence, we can reduce the system to a two-dimensional system in which we keep track only of grass (G) and savanna trees (T) since saplings (S) will be given by $S = 1 - T - G$.

Population-Potential Landscape and Flux Quantification for the SL Model. Due to fluctuations from internal and external sources, the deterministic dynamics described by a set of ordinary differential equations need to be modified to include the contribution of the additional fluctuation forces. Thus, the following stochastic dynamics emerge (4, 10, 37, 39, 40): $d\mathbf{x} = \mathbf{F}(\mathbf{x})dt + \mathbf{g} \cdot d\mathbf{W}$, where $\mathbf{x}$ is the vector representing the observables for the population or species density; and $\mathbf{x} = \{G, T\}$ for the SL model. In our case, $\mathbf{x}$ does not represent spatial variables as we model spatial extent only implicitly by tracking the proportions of space covered by each vegetation type. We retain this notation for both the stochastic dynamics and the corresponding Fokker–Planck equation. $\mathbf{F}(\mathbf{x})$ is the driving force for the dynamics, and $\mathbf{W}$ coupled with the matrix $\mathbf{g}$ represents an independent Gaussian fluctuating process. We set $D\mathbf{G} = (1/2)(\mathbf{g} \cdot \mathbf{g}^{\mathsf{T}})$, where D is a constant describing the scale of the fluctuations and $\mathbf{G}$ represents the diffusion matrix of the fluctuations. In this study, $\mathbf{G}$ is an isotropic diagonal identity matrix, for simplicity, and thus the noise is chosen as Gaussian white noise.

The stochastic dynamics are characterized by the probability distribution of the system state at time t, $P(\mathbf{x}, t)$, which can be obtained by solving the Fokker–Planck equation:

$$\partial_t P = -\nabla \cdot \mathbf{J} = -\nabla \cdot [\mathbf{F}P - (1/2)\nabla \cdot ((\mathbf{g} \cdot \mathbf{g}^{\mathsf{T}})P)]. \quad [2]$$

Hence, the steady-state probability distribution, denoted by P_{ss}, can be obtained by solving the steady-state Fokker–Planck equation; i.e., $\partial_t P = 0$. The normalization condition $G + S + T = 1$ in the SL model means that the system is reduced from three dimensions to two. Therefore, the state space is an isosceles right triangle with the two equal length sides having length 1 (see Fig. 2). In equilibrium systems, the probability follows a Boltzmann distribution $P \sim \exp[-U]$ (1, 4, 10, 41) and the energy U is called the population-potential landscape. Thus, the driving force for the dynamics is determined by the gradient of the population-potential landscape in equilibrium systems.

In nonequilibrium systems, the force $\mathbf{F}$ cannot be written as the gradient of a potential in general. However, the population-potential landscape can still be defined and linked to the probabilities by the formula $U = -\ln P_{ss}$ (1, 4, 31). We denote by $\mathbf{J_{ss}} = \mathbf{F}P_{ss} - D\nabla \cdot (\mathbf{G}P_{ss})$ the corresponding steady-state probability flux and note that it satisfies the divergence-free condition $\nabla \cdot \mathbf{J}_{ss} = 0$.

In equilibrium systems, there is no net flux in or out of the system. Thus, the steady-state probability flux is zero at all points in the state space; this is the so-called detailed balance condition $\mathbf{J}_{ss} = 0$. In nonequilibrium systems, the nonzero flux, $\mathbf{J}_{ss}$, is divergence-free and breaks the detailed balance condition. This nonzero flux thus provides a quantitative measure of the degree to which the system is out of equilibrium. In nonequilibrium ecological systems, the driving force $\mathbf{F}$ can be decomposed into the gradient of the potential U, the curl steady-state probability flux, and the divergence of the diffusion coefficient as $\mathbf{F} = -D\mathbf{G} \cdot \nabla U + \mathbf{J}_{ss}/P_{ss} + D\nabla \cdot \mathbf{G}$. The population potential landscape U and the steady-state probability flux $\mathbf{J}_{ss}$ together can address many global dynamical and thermal dynamical issues including stability, robustness, dynamics, and thermodynamics of ecological systems. We use the SL model under fluctuations to study the stochastic dynamics and the interplay among grass, saplings, and trees (5, 6). We solve the Fokker–Planck partial differential equation given by Eq. **2** for the SL model with reflecting boundary conditions, i.e., $\mathbf{n} \cdot \mathbf{J} = 0$, where $\mathbf{n}$ is a unit vector perpendicular to the boundary of the state space, to obtain the probability distribution of the system. We can thus quantify the population-potential landscape U and the flux $\mathbf{J}_{ss}$, which together determine the driving forces for the dynamics of the ecological system.

Forest–savanna landscapes are nonequilibrium open ecological systems and hence exchange energy with their environments, which leads to dissipation. The entropy of a stochastic system can be defined as $S_{entropy} = -\int P \ln P d\mathbf{x}$ and the change in the entropy in time can be divided into the entropy production rate and heat dissipation rate. The time evolution of the entropy of the system is thus given by $\dot{S}_{entropy} = \dot{S}_t - \dot{S}_e$, where the entropy production rate (EPR $= \dot{S}_t$) is given as $\dot{S}_t = \int d\mathbf{x}(\mathbf{J} \cdot (D\mathbf{G})^{-1} \cdot \mathbf{J})/P$ (31, 42–44). Thus, the EPR is explicitly linked to the flux $\mathbf{J}$. Zero flux would give rise to zero-entropy production, which would correspond to an equilibrium system. However, in practice, nonzero fluxes are likely, corresponding to nonequilibrium systems. A higher flux gives rise to a higher EPR, corresponding to more deviations from equilibrium. This formalism provides a link between nonequilibrium driving force (flux) and nonequilibrium thermodynamic cost, i.e., the EPR.

One can prove that $\dot{S}_t \geq 0$, which leads to the second law of nonequilibrium thermodynamics. $\dot{S}_t$ has the physical meaning of the EPR contributed from both the system $\dot{S}$ and the environment $\dot{S}_e$ as $\dot{S}_t = \dot{S}_{entropy} + \dot{S}_e$. This can be understood as a formulation of the first law of nonequilibrium thermodynamics. The heat dissipation rate from the environment is given as $\dot{S}_e = \int d\mathbf{x}(\mathbf{J} \cdot (D\mathbf{G})^{-1} \cdot (\mathbf{F} - D\nabla \cdot \mathbf{G}))$. The heat dissipation rate can be either positive or negative and can quantify the entropy flow rate from the environment to the nonequilibrium system. When the system is at the steady-state $\dot{S}_{entropy} = 0$, the EPR and the heat dissipation rate are equal (31, 42–44). The EPR and the average flux $\text{Flux}_{av} = \int J d\mathbf{x}$ thus provide global thermodynamic measures for the nonequilibrium systems (4, 17, 31, 43). The mathematical notation and definitions outlined above are summarized in *SI Appendix*, Table S1.

Lyapunov Function for the SL Model under Zero Fluctuations. A Lyapunov function is crucial for quantifying the global stability of ecological systems subject to perturbations. One might use the steady-state probability or the associated population potential to explore the global stability under finite fluctuations. However, the population potential is not a Lyapunov function in general (17) and it is often a challenging problem to find Lyapunov functions for complex nonequilibrium systems. Here we show that the intrinsic potential landscape, ϕ_0, is a Lyapunov function for the ecological dynamics in the zero-noise limit (17, 43).

The probability P can be expanded according to the fluctuation strength D as $P(\mathbf{x}) = \exp(-(\phi_0(\mathbf{x})/D + \phi_1(\mathbf{x}) + D\phi_2(\mathbf{x}) + \cdots))/Z$, where $Z = \int \exp(-U(\mathbf{x}))d\mathbf{x}$. By substituting it into Eq. **2**, we obtain the D^{-1} order expansion of the Fokker–Planck equation, which has the largest contribution to the probability under the zero-noise limit. This yields the Hamilton–Jacobi equation (HJE):

$$H = \mathbf{F} \cdot \nabla\phi_0 + \nabla\phi_0 \cdot \mathbf{G} \cdot \nabla\phi_0 = 0. \quad [3]$$

Table 1. Parameter interpretations and default values

Symbol	Ecological interpretation	Default
β	Savanna sapling birth rate	0.38
μ	Savanna sapling mortality rate	0.2
ν	Adult savanna tree mortality rate	0.1
ω_0	Savanna sapling-to-adult recruitment rate basic value	0.9
ω_1	Savanna sapling-to-adult recruitment rate of sigmoid basic value	0.2
θ_1	Grass cover basic value	0.4
ss_1	Slope of the sigmoid	0.01

ECOLOGY

The time evolution of $\phi_0(\mathbf{x})$ is thus given by $\dot{\phi}_0(\mathbf{x}) = \dot{\mathbf{x}} \cdot \nabla\phi_0 = \mathbf{F} \cdot \nabla\phi_0 = -\nabla\phi_0 \cdot \mathbf{G} \cdot \nabla\phi_0 \leq 0$. The value of $\phi_0(\mathbf{x})$ monotonically decreases along the deterministic trajectories under the zero-fluctuation limit since $\mathbf{G}$ is positive definite. Therefore, ϕ_0 is a Lyapunov function and can be used to quantify the global stability of the systems. Furthermore, ϕ_0 is linked with the steady-state probability and population-potential landscape as $U = -lnP_{ss} \sim \phi_0/D$. The solution ϕ_0 of the Hamilton–Jacobi equation, which is the zero-fluctuation limit of the solution to the Fokker–Planck equation, is called the intrinsic potential of the system (17, 43).

In the zero-fluctuation limit, the force $\mathbf{F}$ can be decomposed into a gradient term and a curl term $\mathbf{F} = -\mathbf{G} \cdot \nabla\phi_0 + (\mathbf{J}_{ss}/P_{ss})|_{D\to 0} = -\mathbf{G} \cdot \nabla\phi_0 + \mathbf{V}$, where $-\mathbf{G} \cdot \nabla\phi_0$ represents the gradient of the nonequilibrium intrinsic potential. We set $\mathbf{V} = (\mathbf{J}_{ss}/P_{ss})_{D\to 0}$ as the intrinsic steady-state flux velocity. $\mathbf{J}_{ss}|_{D\to 0}$ represents the steady-state intrinsic divergence free curl flux due to $\nabla \cdot \mathbf{V} = 0$. From the Hamilton–Jacobi equation, the relationship between ϕ_0 and the intrinsic flux is thus $(\mathbf{J}_{ss}/P_{ss})|_{D\to 0} \cdot \nabla\phi_0 = \mathbf{V} \cdot \nabla\phi_0 = 0$. This implies that the gradient of the intrinsic potential and the intrinsic flux are perpendicular to each other in the zero-fluctuation limit.

Due to the normalization condition in the SL model, the state space becomes an isosceles triangle, making calculation of ϕ_0 very difficult. To overcome this problem, we approximate the Lyapunov function ϕ_0 from the expansion of the potential $U(\mathbf{x})$ for the small diffusion coefficient D as $U(\mathbf{x}) = \phi_0(\mathbf{x})/D + \phi_1(\mathbf{x}) + \ldots$. We applied the linear fit method for the diffusion coefficient D versus the DU to solve the ϕ_0 approximately. We use the data of $0.0002 < D < 0.0005$ to fit a line, which is the diffusion coefficient D versus $D \ln P_{ss}$. Thus, the slope of the line leads to the value of ϕ_0 (43, 45). The results are shown later in this paper. An exact numerical solution of the Hamilton–Jacobian equation for the intrinsic potential landscape ϕ_0 under a specific choice of diffusion matrix mimicking the population evolution dynamics is demonstrated in *SI Appendix*.

Nonequilibrium Thermodynamics, Entropy, Energy, and Free Energy of the General Dynamical Systems under the Zero-Fluctuation Limit and the Finite Fluctuations. In equilibrium systems, we can quantify the equilibrium probability distribution and the partition function as well as the entropy and free energy according to the underlying interacting potential energy. The partition function provides a statistical description for the collection of states in the system. For nonequilibrium systems, the intrinsic potential ϕ_0 can be related to the steady-state probability distribution under the zero-fluctuation limit as $\mathcal{P}_{ss}(\mathbf{x}) = P_{ss}(\mathbf{x})|_{D\to 0} = \exp(-\phi_0/\mathcal{D})/\mathcal{Z}$, where $\mathcal{D} = D|_{D\to 0}$. The partition function $\mathcal{Z}$ is defined as $\mathcal{Z} = \int \exp(-\phi_0/\mathcal{D})d\mathbf{x}$. Thus, $\phi_0 = -\mathcal{D} \ln(\mathcal{Z}\mathcal{P}_{ss})$.

The entropy of the nonequilibrium system under the zero-fluctuation limit can be defined by $\mathcal{S} = -\int \mathcal{P}(\mathbf{x}, t) \ln \mathcal{P}(\mathbf{x}, t)d\mathbf{x}$ (4, 17, 31, 43). The intrinsic energy $\mathcal{E}$ of the nonequilibrium system can be defined as $\mathcal{E} = \int \phi_0 \mathcal{P}(\mathbf{x}, t)d\mathbf{x} = -\mathcal{D} \int \ln(\mathcal{Z}\mathcal{P}_{ss})\mathcal{P}(\mathbf{x}, t)d\mathbf{x}$. Thus, the intrinsic free energy of the nonequilibrium system can be defined as $\mathcal{F} = \mathcal{E} - \mathcal{D}\mathcal{S} = \mathcal{D}\left(\int \mathcal{P} \ln(\mathcal{P}/\mathcal{P}_{ss})d\mathbf{x} - \ln \mathcal{Z}\right)$.

The nonequilibrium intrinsic free energy always decreases since $\frac{d\mathcal{F}}{dt} = -\mathcal{D}^2 \left(\int \left[\nabla \ln(\frac{\mathcal{P}}{\mathcal{P}_{ss}}) \cdot \mathbf{G} \cdot \nabla \ln(\frac{\mathcal{P}}{\mathcal{P}_{ss}})\right] \mathcal{P}d\mathbf{x}\right) \leq 0$ (17, 43). The minimum value of the nonequilibrium intrinsic free energy is $\mathcal{F} = -\mathcal{D} \ln \mathcal{Z}$. This represents the second law of thermodynamics for nonequilibrium systems. Therefore, the nonequilibrium intrinsic free energy is a Lyapunov function and, as we show presently, it can be used to quantify the global stability of the nonequilibrium system.

We also explore the nonequilibrium free energy under finite fluctuations D. The energy $\mathcal{E}$ of the nonequilibrium system under finite fluctuations can be defined as $\mathcal{E} = \int DUPd\mathbf{x}$, and the entropy under finite fluctuations is $S_{entropy} = -\int P \ln Pd\mathbf{x}$. Thus, the free energy under finite fluctuations is shown as $\mathcal{F} = \mathcal{E} - DS_{entropy} = D \int P \ln(P/P_{ss}(\mathbf{x}))d\mathbf{x}$ (17, 43). The nonequilibrium free energy under finite fluctuations also always decreases since $\frac{d\mathcal{F}}{dt} = -D^2 \left(\int \left[\nabla \ln(\frac{P}{P_{ss}}) \cdot \mathbf{G} \cdot \nabla \ln(\frac{P}{P_{ss}})\right] Pd\mathbf{x}\right) \leq 0$ (17, 43). This shows that free energy under finite fluctuations is also a Lyapunov function (17, 43), which can be used to quantify the global stability of the nonequilibrium system.

Kinetic Speed and Dominant Paths between the Stable States. The path-integral approach can be used to identify and quantify the most likely transitions between two stable states. The path-integral formula characterizing the probability of the path from initial state $\mathbf{x}_i$ at $t = 0$ to final state $\mathbf{x}_f$ at time t is given by (17, 32) $P(\mathbf{x}_f, t|\mathbf{x}_i, 0) = \int D\mathbf{x} \exp[-\int dt(\frac{1}{2}\nabla \cdot \mathbf{F}(\mathbf{x}) + \frac{1}{4}(d\mathbf{x}/dt - \mathbf{F}(\mathbf{x})) \cdot (D\mathbf{G})^{-1} \cdot (d\mathbf{x}/dt - \mathbf{F}(\mathbf{x})))] = \int D\mathbf{x} \exp[-A(\mathbf{x})] = \int D\mathbf{x} \exp[-\int L(\mathbf{x}(t))dt]$, where $L(\mathbf{x}(t))$ is the Lagrangian and $A(\mathbf{x})$ is the action for each path on the potential landscapes. The path integral over $D\mathbf{x}$ represents the sum over all possible paths connecting $\mathbf{x}_i$ at time 0 to $\mathbf{x}_f$ at time t. The exponential factor gives the weight of each specific trajectory and the probability of going from $\mathbf{x}_i$ to $\mathbf{x}_f$ is thus the weighted sum over all possible paths. The path integral can be approximated by the path that contributes the most to the weight since the other paths' contributions are exponentially small. We can find the dominant paths with the optimal weights through minimization of the action $A(\mathbf{x})$ or Lagrangian $L(\mathbf{x}(t))$ as the dominant path probability is proportional to $\exp[-A(\mathbf{x})]$. Thus, we can identify the paths that give the largest contribution to the weight as the dominant savanna– forest switching pathways. The path-integral formalism here is based on the Onsager–Machlup functional for a diffusion process under finite fluctuations (46). Under the zero-noise limit, the divergence of the force term in the Onsager–Machlup functional can be ignored. As a result, the path-integral formalism is reduced to the form arising in the Freidlin–Wentzell theory (47).

Ecological Dynamics: The Landscape-Flux Approach versus Conventional Nonlinear Dynamics. We show comparison between conventional nonlinear dynamics analysis and landscape-flux theory in Table 2. In standard deterministic nonlinear dynamics, local stability analysis can be performed and stable states can be identified. However, there is no information about the weights of the states, information that can be provided from the probabilistic landscape-flux approach. Furthermore, local stability analysis does not quantify the connections or switching paths between the stable states, properties that can be quantified through the landscape-flux approach. In addition, conventional nonlinear dynamical analysis often does not provide information about the global stability of a system, typically due to the difficulty in finding a suitable Lyapunov function. The landscape-flux approach can provide a way to identify the Lyapunov function and therefore quantify the global stability.

The additional information that this approach provides is the degree of difficulty in switching from one stable state to another, a property that can have significant ecological consequences in real-world systems. Similarly, while conventional nonlinear analysis can identify the bifurcations for the system, there is typically no information about how the bifurcations occur and the possible origins of such bifurcations. This is one of the most important unresolved issues in theoretical ecology and can be addressed in the landscape-flux approach by searching for the physical (dynamic and thermodynamic) origins of the bifurcations of the ecological systems.

Table 2. Comparison between conventional nonlinear dynamics analysis and landscape-flux theory

Conventional nonlinear dynamics	Landscape-flux approach
Locations of the fixed-point states	Weights of the states
Local dynamics around fixed points	Global connections between the fixed-point states
Stochastic local stability analysis	Global stability analysis based on landscape and flux under fluctuations
Deterministic local stability analysis	Lyapunov function identifications for quantifying global stability under no fluctuations
Isolated fixed points	Barrier height between the local stable states
Fixed points with no kinetic connections	Kinetic rates of switching between the local stable states
Fixed points without the connected paths	Dominant kinetic pathways and associated weights between local stable states
Locations of the bifurcations	Physical origins and predictions of bifurcations
Locations of bifurcations	Kinematic markers and early warning signals of the bifurcations
No identification of the driving force components	Theoretical framework of the driving force via landscape and flux

In deterministic nonlinear dynamics, the driving force in the model is simply the right-hand side of the evolution equations. However, there is usually no easy way to understand the nature of this driving force when the system is subject to noise. The landscape-flux approach offers a framework to study the stochastic dynamics by identifying the driving force as the action of both the landscape gradient and rotational flux. One can also quantify the associated global thermodynamics in terms of the EPR. Therefore, the landscape-flux approach provides a general framework to study the global dynamics and thermodynamics of the ecological systems. Finally, in deterministic nonlinear dynamics, the stable states emerge from the interactions. However, in the presence of stochastic forcing, new quasi-stable states can emerge, and these new states can be predicted by the landscape-flux approach.

Results

Dynamics and Thermodynamics via Potential-Flux Landscapes.

Nonequilibrium population-potential landscape and flux with finite fluctuation. We now illustrate the landscape-flux approach to ecological dynamics by studying the SL model under finite fluctuations. Savanna denotes a grass-dominated state with some trees and saplings, while forest is a tree-dominated state with few grasses and saplings. The grassland state has no saplings or trees present.

Fig. 1*A* shows the deterministic phase diagram in β (the sapling birth rate), while Fig. 2 shows two-dimensional population-potential landscapes (U) for a range of βs with $D = 0.0001$; in both cases the system is considered under finite fluctuations. In Fig. 2, the population-potential landscape initially has one stable state that evolves from the grassland state [i.e., $(G, T) = (1, 0)$] to the savanna state with increasing β. As β increases further, the stable forest state emerges. As β increases, the ecological system switches from savanna dominant to forest dominant (also shown in Fig. 1*A*), and as β increases further, the grass is completely invaded by the trees due to the high sapling birth rate. Eventually, the forest state becomes dominant while the savanna state disappears. Fig. 3 shows the fluxes on the population-potential landscapes as white arrows for increasing β. To show the fluxes clearly, we give only the directions of the larger values of the fluxes, which are all around the stable states. Vegetative growth factors, such as nutrition and energy from soil, air, water, and sunshine, will vary due to different climates in the environment. Thus, when the system has two stable states savanna and forest, the fluxes originating from the vegetative growth factors go around the stable states, enhancing their communications to each other. In Fig. 3, the negative gradient of the population-potential landscapes and the nonzero flux are the driving forces of the forest–savanna ecological system.

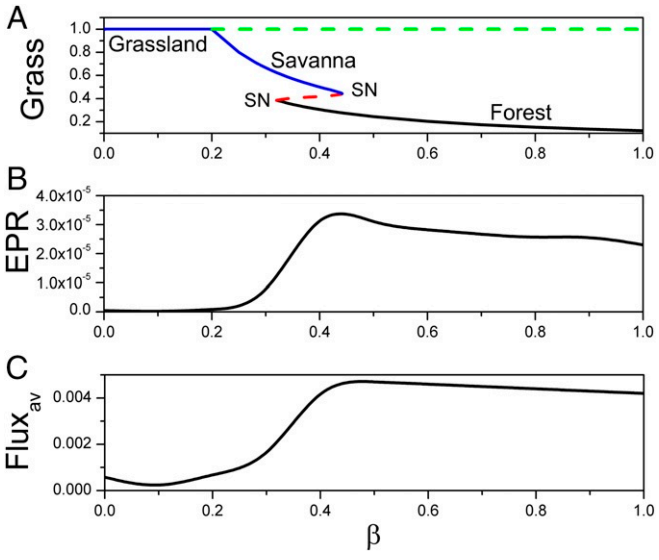

Fig. 1. (*A*) The phase diagram versus β. (*B*) The population entropy production rate versus β. (*C*) The population average flux versus β.

Fig. 3 shows the dominant population paths, calculated under finite fluctuations, on the population-potential landscape U with different parameters. Once more, savanna and forest are the two stable states. The red line is the dominant population path from forest state to savanna, while the thick white line is the dominant population path from savanna state to forest. The white arrows represent the steady-state probability fluxes that guide the dominant population paths deviating from the naively expected steepest-descent path passing through the saddle point based purely on the population-potential landscape. Therefore, the dominant population paths from savanna to forest and the dominant population paths from forest to savanna do not follow the same path, in contrast to the equilibrium case under zero flux. The two dominant population paths are different, which shows the irreversibility of the dominant population paths due to the presence of the nonequilibrium rotational flux. Thus, the dominant population paths going from savanna to forest (the white lines) and going from forest to savanna (the red lines) will follow different routes. The two dominant population paths under larger fluctuations (bigger diffusion coefficient D) are shown in Fig. 3*D*; the two dominant population paths are also apart from each other due to presence of the steady-state probability fluxes such as those shown in Fig. 3*C*. The fluxes have spiral shapes around these two basins, which shows the dynamic nature of the nonequilibrium system.

The red and white lines approximately form a figure-"8" shape, emphasizing that the switching dominant population paths are distinct and thus that the transition is "irreversible." The white path lines start from savanna and initially the flux force is in the counterclockwise direction, as shown in Fig. 3. Therefore, the dominant population paths from savanna to forest initially move upward under the action of the flux force compared to the paths based purely on the gradient of the landscape. When the grass G decreases close to $\theta_1 = 0.4$, the savanna sapling-to-adult recruitment rate $\omega(G)$ will run into a threshold value and increase sharply. Therefore, the white path lines arrive at their inflection point, where the flux changes direction to be clockwise. As a result, the white path moves downward from then on under the action of the flux force, compared to the paths based purely on the gradient of the landscape. Similarly, the red path line starts from the forest state and initially the flux force is in the clockwise direction, as shown in Fig. 3. Therefore, the dominant population paths from forest to savanna states initially move more upward under the action of the flux force. When the grass G increases close to $\theta_1 = 0.4$, the savanna sapling-to-adult recruitment rate $\omega(G)$ hits its threshold value and decreases sharply. The red path lines arrive at their inflection point, where the flux becomes counterclockwise. The red path moves downward from then on due to the action of the flux. In ecological terms, this finding is quite intuitive. For a forest to establish, trees must first establish as saplings, whereas they need not regress into saplings before dying, such that the composition of the system is quite different as a forest opens up compared to when a savanna closes over (see ref. 48 for empirical evidence supporting this mathematical intuition).

The weight of the population path represents the probability of each route for state switchings under finite fluctuation. It can be used to quantify the likelihood of different routes for the transition between savanna and forest. The dominant population path probability can be quantified by the population action $A_{po}(\mathbf{x})$ as shown in *SI Appendix*, Fig. S1 (β, μ, θ_1) and *SI Appendix*, Fig. S22 (ν, ω_0, ω_1). Bigger population action denotes lower dominant population path probability since the dominant population path probability is proportional

ECOLOGY

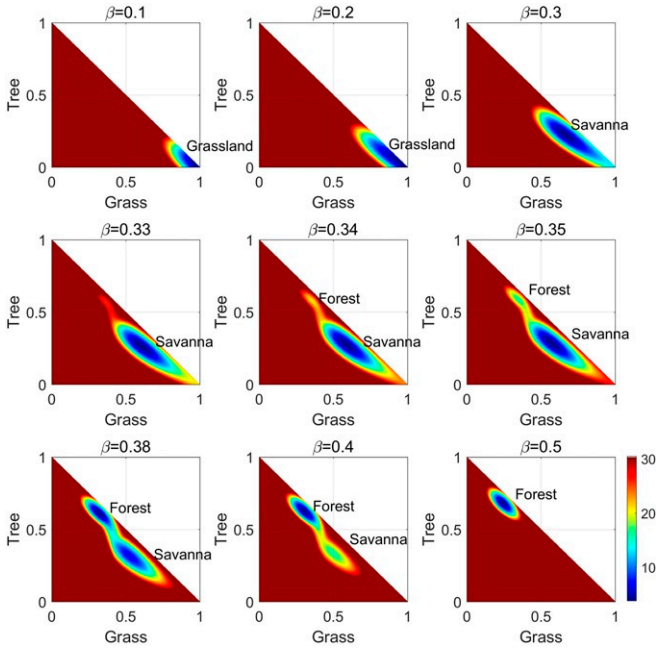

Fig. 2. The two-dimensional population-potential landscapes versus β with finite fluctuation $D = 0.0001$.

to $\exp[-A_{po}(\mathbf{x})]$. As β becomes larger, the probability of the dominant population path from forest to savanna decreases, while the probability of the dominant population path from savanna to forest increases. The variation of the population-potential landscape, the flux, the population actions, and the dominant population paths in $\mu, \theta_1, \nu, \omega_0, \omega_1$ are presented in *SI Appendix*.

The intrinsic potential landscape and flux velocity in the zero-fluctuation limit. Fig. 4 shows the three-dimensional nonequilibrium intrinsic potential landscape ϕ_0 with increasing β. The intrinsic potential landscape changes from a dominant savanna stable state, to a savanna and forest coexisting stable state, and then to a dominant forest stable state as β increases. The intrinsic flux and the negative gradient of the intrinsic potential landscape $-\nabla\phi_0$ are in fact perpendicular to each other and the two dominant intrinsic paths, calculated under the zero-fluctuation limit, both pass through the saddle point denoted by the black dot; these facts can also be seen clearly in *SI Appendix*, Fig. S2 via a two-dimensional (2D) projection.

The dominant intrinsic path probability can be quantified by the intrinsic action $A_{in}(\mathbf{x})$ shown in *SI Appendix*, Fig. S3 (β, μ, θ_1) and *SI Appendix*, Fig. S25 (ν, ω_0, ω_1). The results of the intrinsic actions have the same tendencies as those of the population actions.

Throughout the main text and in *SI Appendix*, sections 1–6, the diffusion matrix $\mathbf{G}$ is an isotropic and homogeneous diagonal matrix. In *SI Appendix*, section 7, we present results for certain anisotropic and inhomogeneous fluctuations characterized by different choices of diffusion matrices. We perform a coordinate transformation from a special diffusion matrix in an isosceles triangle into an inhomogeneous diagonal matrix in a square (*SI Appendix*, Fig. S43). Thus, we can numerically solve the Hamilton–Jacobi equation in a regular square shape with the resulting diagonal matrix (17, 43). Results for the anisotropic and inhomogeneous fluctuations are qualitatively similar to those for the isotropic and homogeneous diffusion matrices (*SI Appendix*, Fig. S44).

Barrier heights and kinetic rates of switching between states. Fig. 5*A* shows the barrier heights of the population-potential landscape under finite fluctuations as a function of β. The barrier heights of the intrinsic potential landscape under zero fluctuations versus β are shown in *SI Appendix*, Fig. S5*A*. ΔU_F represents the barrier height from forest to savanna and ΔU_S represents the barrier height from savanna to forest. $\Delta\phi_{0F}$ represents the intrinsic barrier height from forest to savanna, while $\Delta\phi_{0S}$ represents the intrinsic barrier height from savanna to forest.

As expected, population barrier height ΔU_F and intrinsic barrier height $\Delta\phi_{0F}$ increase, while ΔU_S and $\Delta\phi_{0S}$ decrease as β increases. High barrier height from the bottom of the basin of the attraction to the barrier top implies that it is difficult to escape from the basin of attraction of that state. Therefore, larger ΔU_F indicates that the forest state is more stable while larger ΔU_S indicates a more stable savanna state. As the sapling birth rate β increases, the trees become more established and the forest state becomes more stable, while the savanna state becomes less stable. The forest–savanna system thus switches from savanna dominance to forest dominance for β sufficiently large. The barrier heights of the population-potential landscape and the intrinsic barrier heights of the intrinsic potential landscape have almost the same qualitative features (cf. Fig. 5*A* and *SI Appendix*, Fig. S5*A*). The barrier heights of the population-potential landscape and the intrinsic potential landscape as functions of β, μ, θ_1, ν, ω_0, and ω_1 are shown in *SI Appendix*, Figs. S4 and S5.

Due to stochastic fluctuations or other external forces, ecological systems may not stay in the basin of attraction of their current stable state, but may escape from this basin, switching the system to an alternative stable state. Mean first passage time (MFPT) is the average time for a stochastic process to reach a given threshold value (state) for the first time. The MFPT can be used to quantify the kinetic speed or kinetic time for switching from one state to another, both natural measures for the tendency of the system to escape its current basin of attraction. We use Langevin dynamics to simulate the stochastic SL model and study the distribution of the MFPT from one stable state to another as follows: We choose one stable state as the initial condition and a disc of radius $r_0 = 0.01$ around the other stable state serves as the target final "state." We then collect statistics of the first passage time from the initial state to the final state before averaging over all simulations to compute the mean first passage time (40,000 simulations were performed to obtain the results shown). τ_{SF} is the MFPT from savanna to forest while τ_{FS} is the MFPT from forest to the savanna. We show the logarithm of MFPT versus β in Fig. 5*B* and observe that $\ln\tau_{SF}$ decreases and $\ln\tau_{FS}$ increases as β increases. In other words, it becomes easier to switch from savanna to forest and harder to switch from forest to savanna as the sapling birth rate increases.

The population-potential landscape topography, quantified by the barrier height, and the corresponding logarithm of MFPT have positive correlation and are shown in Fig. 5*C*. Thus, from the barrier height ΔU_F, ΔU_S and the logarithm of the corresponding MFPT, $\ln\tau_{FS}$, one can see that the MFPT is directly related to ΔU_F. Thus, $\ln\tau_{SF}$ has a correlation with the barrier height ΔU as $\tau \sim exp(\Delta U)$. This shows that the higher the barrier height or the deeper the valley is, the longer time it takes to escape from the valley. This indicates that the population-potential landscape topography is often correlated to the kinetic speed of the state switching and therefore the communication capability for the global stability of the ecological system. We can also see that kinetic speed can sometimes be estimated based on the population-potential landscape topography through the barrier heights. The logarithm of MFPT versus other parameters and the logarithm of MFPT versus barrier heights are presented in *SI Appendix*, Fig. S6 (β, μ, θ_1) and *SI Appendix*, Fig. S26 (ν, ω_0, ω_1). We also found the barrier height ΔU_F, ΔU_S and

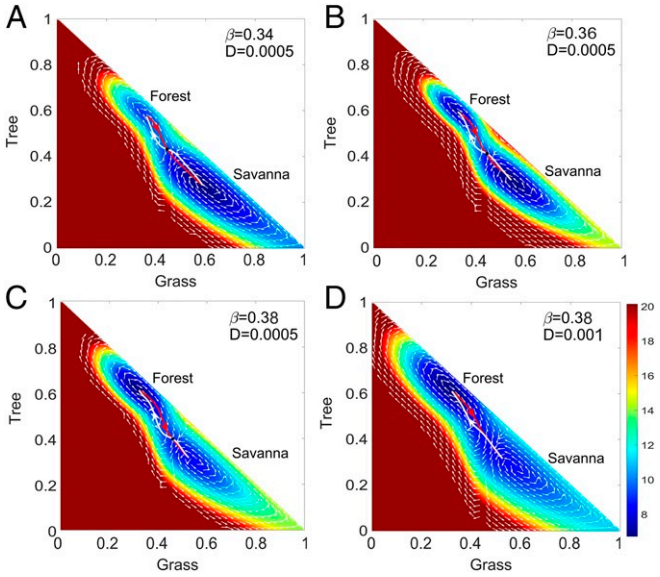

Fig. 3. (*A–C*) The dominant population paths and fluxes on the population-potential landscape U with different $\beta = 0.34, 0.36, 0.38$ and $D = 0.0005$. The white lines represent the dominant population paths from the savanna state to the forest state. The red lines represent the dominant population paths from the forest state to the savanna state. The white arrows represent the steady-state probability fluxes. (*D*) The dominant population paths and fluxes on the population-potential landscape U with $\beta = 0.38$ and $D = 0.001$.

the corresponding MFPT $\ln \tau_{FS}$, $\ln \tau_{SF}$ have the correlation of $\tau \sim \exp(\Delta U)$ (*SI Appendix*).

Early warning signals for bifurcations. Many complex systems, from ecological systems to financial markets and climates, have tipping points when the systems evolve into a critical dynamic regime. Predicting the system behavior before it reaches a tipping point is extremely difficult, but recent studies in different fields suggest that common early warning signals may be tracked. For a range of different types of systems, these signals can be used to detect whether the critical threshold is approached. When one phase state changes to another, the dispersed fluctuations that occur in the phase transition from an old state to the new state not only increase in magnitude, but also extend in duration. This lengthening of time is called "critical slowing down" in statistical physics. The closer the system is to the critical state of sudden change, the more significant this slowing down will be (49, 50). We briefly illustrate how these concepts and techniques can be applied to the SL model in both the finite-fluctuation case and the zero-fluctuation limit.

Finite fluctuations. There are two phase transition points for this set of parameters, as shown in Fig. 1*A*. Fig. 1*B* shows the population entropy production rate versus β. Fig. 1*C* shows the population average flux versus β. As β increases, population Flux_{av} and population EPR both increase markedly before then decreasing slightly. Furthermore, both the population averaged flux and population entropy production rate undergo significant changes at the saddle-node bifurcation shown in Fig. 1*A*. When undergoing a critical transition at the saddle-node bifurcation, the system has two coexisting stable states in the phase transition region emerging from one stable state. For nonequilibrium systems, while the gradient force always tends to stabilize the point attractor, the flux force (due to its rotational nature) will tend to destabilize the existing state, but stabilize the flow between the states. Therefore, there is a possibility of a new state emerging for the purpose of stabilizing the flow between the existing state and this newly formed state. Thus, the stability of the coexisting state is not determined by the individual state but by the associations between the two states. In this sense, the two states in the transition region have associations with each other, in contrast to the individual state, and more state space can be explored under fluctuations. The system appears to require more average flux to maintain the coexisting states and their associations, in contrast to when there is only one stable state. This also results in greater thermodynamic cost or dissipation. These effects lead to the peaks in the bifurcation region in EPR and Flux_{av}. We show the population entropy production rate and the population average flux versus other parameters in *SI Appendix*. Both the population average flux and the population entropy production rate have significant changes near (between) the two saddle-node bifurcations under different parameters and their associated changes, reaching similar conclusions to those above.

The forest state has higher EPR and Flux_{av}, which implies that the trees need more vegetative growth factors and more nutrition and energy than grass from the savanna environment. The savanna needs fewer vegetative growth factors, less nutrition, and less energy than trees from the environment. The population Flux_{av} and population EPR have similar changes with respect to β, as shown in Fig. 1 *B* and *C*. Hence population Flux_{av} and EPR may provide warning signals of bifurcations. Therefore we may use the population Flux_{av} and EPR to explore the global stability and bifurcations of the nonequilibrium ecological dynamics.

Long-time trajectories of the SL model with the default values of the parameters and $D = 0.0005$ are shown in Fig. 6*A* to illustrate this noise-induced attractor switching from a pathwise perspective. The average of the differences between the two-point cross-correlations forward and backward in time can be used to measure the time irreversibility and there-

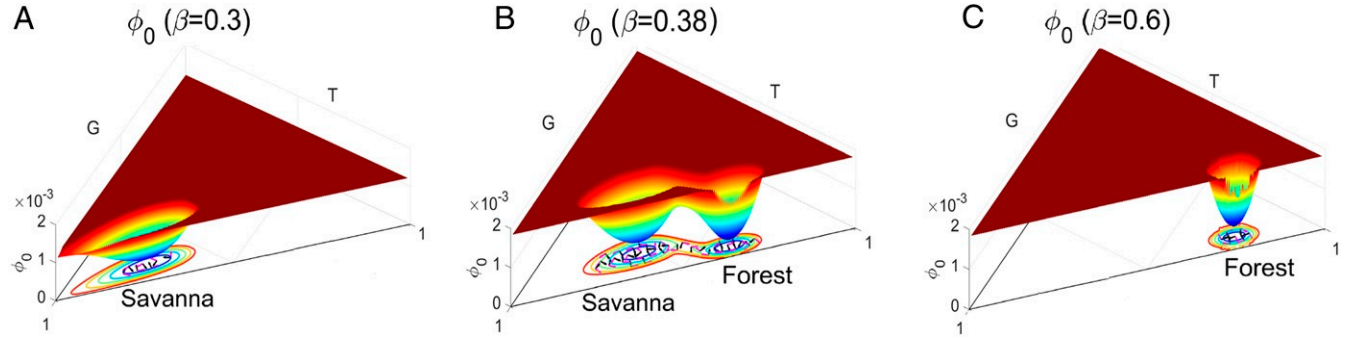

Fig. 4. The three-dimensional intrinsic potential landscape ϕ_0 for increasing β in the zero-fluctuation limit. (*A–C*) The projection of the flux velocity (purple arrows) and the negative gradient of the intrinsic potential landscape $-\nabla\phi_0$ (black arrows) on the intrinsic potential landscape ϕ_0 for increasing β.

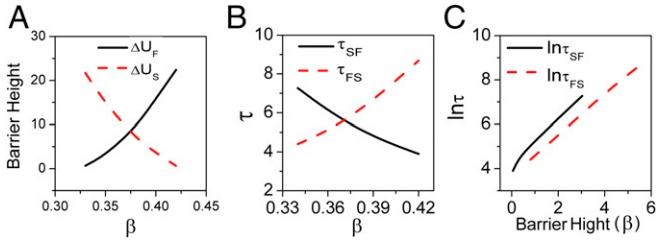

Fig. 5. (*A*) The population barrier heights versus parameter β. (*B*) The logarithm of MFPT versus β. (*C*) The logarithm of MFPT versus barrier heights for β.

fore the degree of detailed balance breaking (36, 51, 52). The cross-correlation function is defined as $C_{XY}(\tau) = \langle X(0)\, Y(\tau)\rangle = \sum X^i\, Y^j\, P_i^{ss}\, P_{ij}(\tau)$, where X and Y denote the time trace signals of variables X and Y. P_i^{ss} represents the steady-state probability at state i and $P_{ij}(\tau)$ represents the probability from state i to state j with time interval τ (51, 52). The nonequilibrium steady-state probability flux, J_{ij}^{ss}, is defined as $J_{ij}^{ss} = P_i^{ss} k_{ij} - P_j^{ss} k_{ji}$, since $\tau P_{ij}(\tau) \sim k_{ij}\tau$ for small time interval τ, where k_{ij} denotes the transition rate from state i to state j, while k_{ji} denotes the transition rate from state j to state i. The difference between the forward cross-correlation function $C_{XY}(\tau)$ in time and the backward cross-correlation function $C_{YX}(\tau)$ in time is given by (51, 52) $C_{XY}(\tau) - C_{YX}(\tau) = X^A\, Y^B [P_A^{ss} P_{AB}(\tau) - P_B^{ss} P_{BA}(\tau)] = X^A\, Y^B\, J_{AB}^{ss}\tau$, where $J_{AB}^{ss} = \frac{1}{X^A Y^B} \lim_{\tau\to 0} \frac{C_{XY}(\tau) - C_{YX}(\tau)}{\tau}$.

The difference between the cross-correlation functions forward in time and backward in time can quantify the time irreversibility and flux in ecological systems. We use the average difference in cross-correlations $\Delta CC = \sqrt{\frac{1}{t_f}\int_0^{t_f} (C_{XY}(\tau) - C_{YX}(\tau))^2 d\tau}$, which can measure the difference in cross-correlation functions between forward in time and backward in time with different sets of parameters as shown in Fig. 6*B* and *SI Appendix*, Fig. S40. The forward in time cross-correlation function and the backward in time cross-correlation function are equal to each other with zero flux (52). Thus, the average difference of cross-correlation functions ΔCC can be used to quantify the flux and therefore the degree of the time irreversibility or the detailed balance breaking (36, 51, 52). Importantly, this provides a practical method to quantify one part of the dual driving force of the ecological system from cross-correlations between the real time trajectories of the empirical observations of the variables of interest in ecological systems. Along with the earlier finding in this study, we can quantify both driving forces of the ecological system: the landscape from the frequency statistics or distribution of the variables and the flux from cross-correlations between real time trajectories from the empirical observations of ecological dynamics. As detailed in *SI Appendix*, the average difference of cross-correlations has almost the same trends with respect to different parameters as the Flux_{av} and EPR. Crucially, the average differences in cross-correlations become significantly higher near (between) the two saddle-node bifurcation regions. This provides a possible practical way to infer the onset or offset of the bifurcation from the observed time traces of the ecological systems, giving rise to a possible early warning signal.

The distributions of grass and trees in the state space are shown for various values of β in Fig. 7 *A–C* and we observe the expected change from savanna to forest dominance as β increases. The variances of grass and trees versus various parameters are also shown in Fig. 7*D* for β and *SI Appendix*, Fig. S41 for other parameters. The variances of grass, σ_S, and the variances of trees, σ_F, all have peaks near (between) the two saddle-node bifurcations for each parameter. Thus, the variances from the empirical observations of the ecological dynamics can also provide a possible early warning signal for the onset of a bifurcation.

The logarithms of the variances of the kinetic first passage time from savanna to forest $\log(\sigma_{SF})$ and the logarithms of the variances of the kinetic first passage time from forest to savanna $\log(\sigma_{FS})$ and their sum $\log(\sigma_{SF} + \sigma_{FS})$ are shown in Fig. 7*E* for β and *SI Appendix*, Fig. S42 for other parameters. For one stable savanna state, we calculate the first passage time from a certain point near the forest state determined in the two-state parameter regime to the savanna state. In reverse, we can obtain the first passage time for one stable forest state. Both $\log(\sigma_{SF})$ and $\log(\sigma_{FS})$ monotonically increase or decrease as the parameter changes. This indicates that the more stable the states are, the larger the variances of the first passage time will be. The sums of the variances have a "U" shape, indicating that when the ecological system has two stable states coexisting, there are fewer fluctuations in its kinetics. When the barriers for the two stable states have very different heights, the deeper one (the more stable one) has the larger variance of the escape times and is dominant in the sums of the variances of the escape times for the two stable states. When the barriers for the two stable states are nearly equal in height, the sum of variances of the escape times for the two states reaches the minimum compared to the cases of the unequal barrier heights. This is because the communication between the two states in the two-state coexisting case is much more frequent than that in the one stable state alone. While the gradient always tends to stabilize the point attractors, the flux tries to destabilize the point attractor, but stabilizes the flow between the stable states. Thus, the flux flow between the two stable states drives the stability of the state coexistence. The sum of the variance of the kinetic first passage times forward and backward has significant changes near (between) the two saddle-node bifurcation regimes. This shows that through the real time trace analysis of the ecological dynamics, one can use the fluctuations in kinetics to quantitatively locate where the bifurcation will be likely to occur, thus providing a possible early warning signal.

The zero-fluctuation limit. There are two phase transition points for the set of parameters we considered, as shown in Fig. 8*A*. Fig. 8*A* is the same as Fig. 1*A* since it is convenient to check the transition zone and compare it with the other plots. Fig. 8*B* shows the intrinsic entropy production rate versus β, while Fig. 8*C* shows the intrinsic average flux versus β. As β increases, inEPR and inFlux_{av} both increase first and then decrease. Both inFlux_{av} and inEPR have significant changes along with the bifurcation shown in Fig. 8*A*. We also found that the forest has more inEPR and inFlux_{av}, which implies that the trees need more vegetative growth factors and cost more nutrition and energy from the savanna environment. While the savanna needs fewer vegetative growth factors and costs less nutrition and energy from the savanna environment. The peaks in the inEPR and the inFlux_{av}

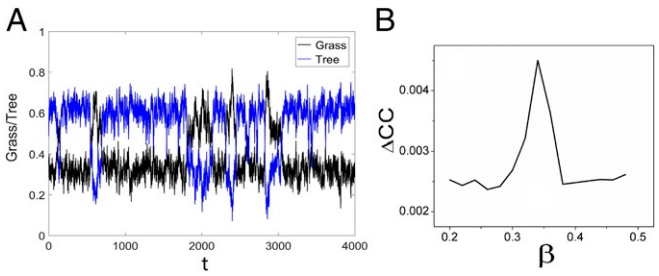

Fig. 6. (*A*) The trajectories of grass and trees. Shown is the average change of the forward and backward in time cross-correlation function ΔCC as a function of parameter β (*B*).

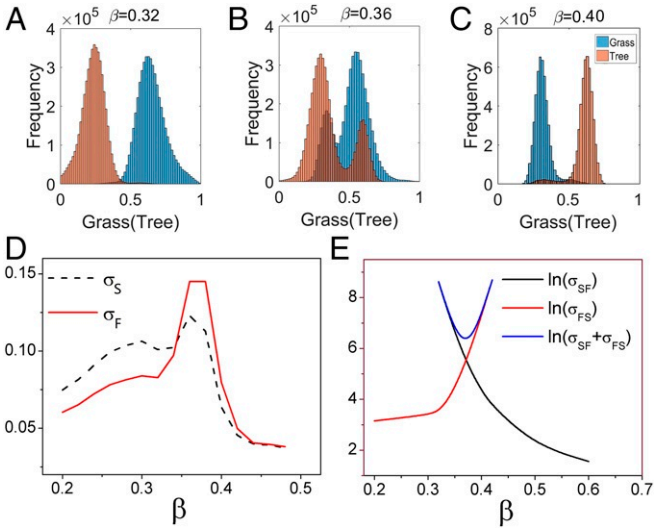

Fig. 7. The frequencies of *Grass* and *Tree* along the variable state space with $\beta = 0.32$ (*A*), 0.36 (*B*), 0.40 (*C*). (*D*) The variances *Grass* σ_S and the variances *Tree* σ_F versus β. (*E*) The logarithms of the variances of the first passage time from *Savanna* to *Forest* log(σ_{SF}) and the first passage time from *Forest* to *Savanna* log(σ_{FS}), and the logarithms of the sum of them log($\sigma_{SF} + \sigma_{FS}$) versus β.

are distinct at the phase transition region. This shows that the inEPR and the inFlux_{av} may be used to characterize the fundamental properties of the system, such as bifurcations. Both the inEPR and the inFlux_{av} under zero fluctuations have more significant changes near (between) the two saddle-node bifurcation regions than those of population entropy production and population flux under finite fluctuations.

However, the critical slowing-down theory applies only to the continuous phase transition (often called second-order phase transition) and hence for the discrete phase transition (such as first-order phase transition) we cannot use critical slowing down to trace the bifurcation signals. From this study and some others (36), EPR and Flux_{av} can both be used as possible early warning signals or markers for bifurcations such as subcritical pitchfork bifurcation and supercritical pitchfork bifurcation, as well as saddle-node bifurcation. Both EPR and Flux_{av} are not constrained to only be markers for continuous transitions. In fact, they apply to both discrete and continuous transitions in the examples shown. We suggest that the above statement may be general. Therefore, this may provide a feasible way to predict the bifurcations in ecological systems to avoid catastrophic change.

EPR and Flux_{av} are observed to have extreme values between the two saddle-node bifurcations as the parameter varies. The locations of these peak values in EPR and Flux_{av} are close to the place where the two stable states are equal in chances (probabilities) of appearance (Figs. 2, 4, and 8). This is because the emergence of two stable states and their associated connections needs more consumptions to maintain in contrast to that of the one individual state. Away from the extreme values in average flux and entropy production or equal probability of the two states, the system switches the dominance of the stability on the landscapes (Figs. 2 and 4). Thus, near the regime of the coexistence of the two stable states, the former stable state becomes less stable while the former less stable state becomes more stable when the system goes through the regime with extreme values of EPR and Flux_{av} or equal basin depths of the two stable states (Figs. 2 and 4). It will then be easier to switch from the former stable state to the latter stable state. Since the EPR and Flux_{av} change significantly upward before their peak values, they provide possible early warning signals for the bifurcations or more explicitly the switching in the dominance of the stabilities from one state to another (Figs. 2, 4, and 8).

Fig. 8*D* shows the intrinsic free energy versus β. The slope of the nonequilibrium intrinsic free energy significantly changes near the phase transition zone, although the nonequilibrium intrinsic free energy is continuous. Fig. 8 *B–D* shows that significant slope changes in intrinsic entropy production rate, intrinsic average flux, and intrinsic free energy (analogous to the equilibrium case) may provide signals of bifurcation. The nonequilibrium intrinsic free energy may also be useful to quantify the global phases of the system and the bifurcations. Therefore, we may use this nonequilibrium intrinsic free-energy function as well as the intrinsic Flux_{av} and intrinsic EPR to explore the global stability and bifurcations of the nonequilibrium ecological dynamics.

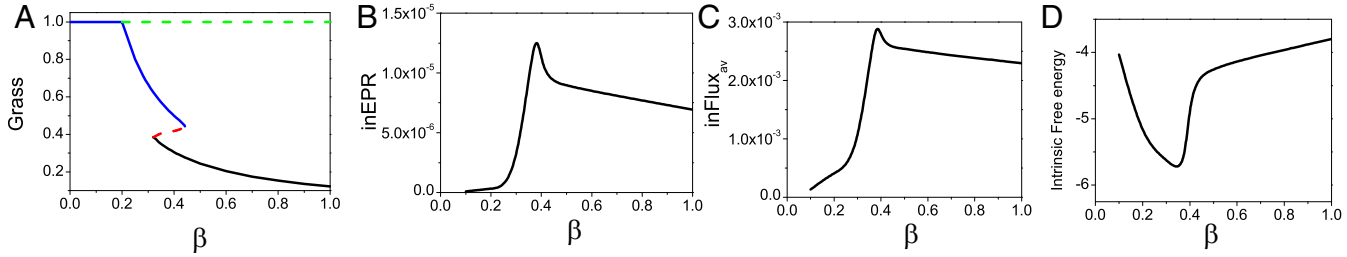

Fig. 8. (*A*) The phase diagram versus β. (*B*) The intrinsic entropy production rate versus β. (*C*) The intrinsic average flux versus β. (*D*) Intrinsic free energy versus β.

Stochastic Fluctuations Generate a New Stable State. Fig. 9*A* shows the deterministic phase diagram mapping the fraction of grass cover versus μ. When the savanna saplings mortality rate is very small, the only stable state is forest, but as μ is increased, the dynamics shift from forest to savanna. For μ between about 0.14 and 0.37, bistability emerges and beyond 0.37, the dynamics approach a state dominated by grass. As μ increases further, trees occasionally go extinct and a new quasi-stable grassland state emerges. For μ larger than 0.37 but less than 0.65, the grassland state is always stable on the G axis and unstable on the T axis. For μ beyond 0.65, this state becomes stable. Fig. 9*B* shows the corresponding stochastic phase diagram versus μ with $D = 0.0001$ (see *SI Appendix* for further details on the stochastic phase diagram). Remarkably, the grassland state becomes quasi-stable much sooner than stable in the deterministic phase diagram (around $\mu = 0.3$) in the presence of stochastic fluctuations.

Fig. 10 *A* and *C* shows three-dimensional population-potential landscapes varying with increasing savanna saplings mortality rate μ with $D = 0.0001$. Fig. 10 *B* and *D* shows the magnification of Fig. 10 *A* and *C* with lower cutting maximum values. Fig. 10 *B* and *D* show the details around the grassland state $[1, 0]$. For $\mu = 0.3$, as in Fig. 10*A*, the system has two stable fixed points in its deterministic phase diagram (Fig. 9*A*) and three stable fixed points in its stochastic phase diagram (shown in Fig. 9*B*); the grassland state $[1, 0]$ is not a stable fixed point for the deterministic SL model for this value of μ. We can see from Fig. 10*D* that the grassland state is a stable state with a very small basin in stochastic dynamics when $\mu = 0.3$. Fig. 10 *C* and *D* shows the population-potential landscape with $\mu = 0.35$. The population-potential landscape around $[1, 0]$ shows that the grassland state has a relatively small basin of attraction, but this basin is larger than that shown in Fig. 10*A*, indicating that the basin of the grassland state becomes deeper as μ increases.

The emergence of the grassland state in Fig. 10, leading to the coexistence of the three stable states forest, savanna, and grassland, contrasts with the deterministic dynamics that predict the absence of forest extinction. The newly quasi-stable grassland state is thus born from the stochastic fluctuations. An important prediction of the landscape-flux approach is the emergence of new quasi-stable states due to fluctuations. Fig. 10 highlights this effect, where the deterministic system predicts the existence of only two stable states (forest and savanna; Fig. 9*A*) and the stochastic system displays an additional quasi-stable grassland state (see Figs. 9*B* and 10, for $0.30 < \mu < 0.37$). Grassland is thus

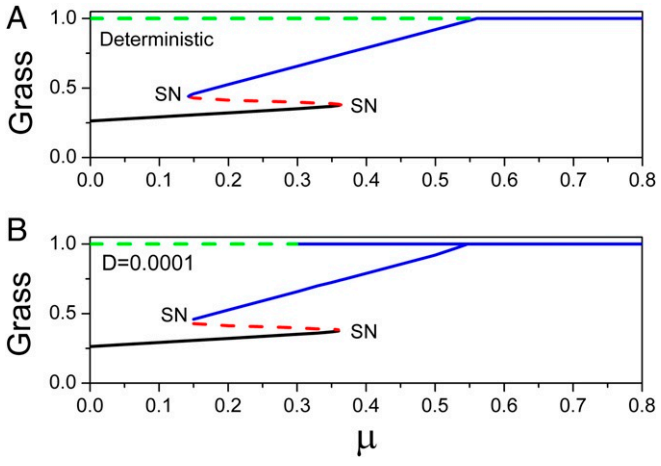

Fig. 9. (*A*) Deterministic phase diagram in μ. (*B*) Stochastic phase diagram (minima of the population-potential landscape) in μ with $D = 0.0001$.

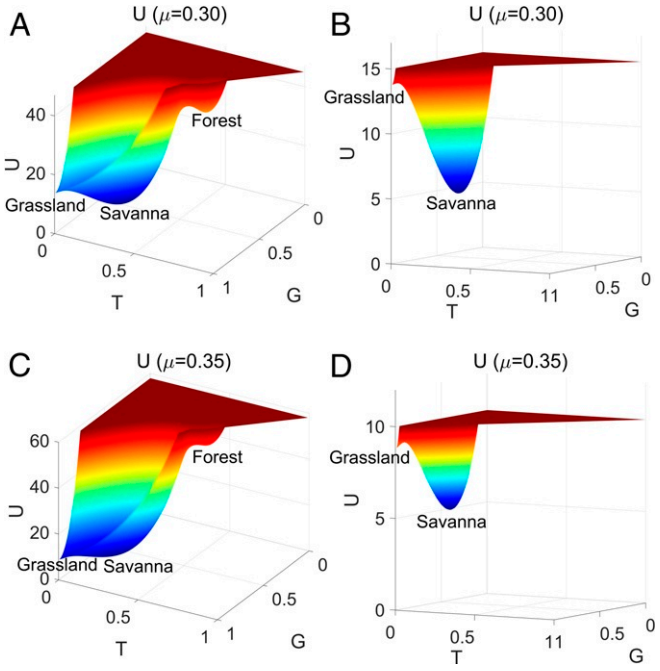

Fig. 10. (*A* and *C*) The three-dimensional population-potential landscapes versus (*A*) $\mu = 0.3$ and (*C*) $\mu = 0.35$. *B* and *D* are the magnification basin of *A* and *C* with lower maximum values.

an unstable fixed point in deterministic dynamics that is stabilized by the fluctuations, and a basin of attraction emerges in its vicinity (see magnification Figs. 10 *B* and *D*). As μ increases, the grassland basin becomes much deeper and thus the associated state becomes more attractive while the savanna state becomes a much shallower minimum of the population-potential landscape and thus less stable.

In the deterministic case, the grassland state is stable in the G direction and unstable in the T direction. However, the constraint $G + T + S = 1$ and the boundary conditions $\{G > 0, T > 0\}$ effectively mean there are three reflecting walls to constrain the system in a specific region. In particular, at $[1, 0]$, the deterministic system is stable in the G direction but also not freely movable in the T direction. The noise effectively expands the accessible region near the point $[1, 0]$. Since there are two walls with infinite potential at $T = 0$ and $G + T = 1$ near $[1, 0]$, the population-potential landscape in the T direction must go up toward both the $T = 0$ wall and the $G + T = 1$ wall. This leads to an effective quasi-stable region or basin of attraction in the T direction, in addition to that already present in the G direction near $[1, 0]$. Thus, the phase space around $[1, 0]$ changes from a saddle-point region to a stable basin due to the dual actions of the noise and boundary conditions.

Conclusion and Discussion

The dynamics of ecological systems are determined by both the population potential, which drives the system toward the potential minimum, and the curl flux, which describes the switching dynamics between basins of attraction. The population-potential landscape can be obtained from the frequency distribution of the observables at long times and can provide insights on the global stability. The steady-state probability flux has divergent free-curl nature and provides the driving force for the nonequilibrium part of the dynamics. Stability is crucial for exploring the function and robustness of an ecological system, but this is a challenging issue both theoretically and practically. Ecological stability is commonly defined as Lyapunov stability, which can describe the global stable behavior of the system under

perturbations. However, it is difficult to obtain a Lyapunov function for complex ecological systems. We introduced a general method to calculate the underlying intrinsic potential landscape as a Lyapunov function that can quantify the global stability of ecological systems. In particular, the intrinsic potential landscape ϕ_0 is shown to be a Lyapunov function in the zero-noise limit.

We investigate the SL model with the underlying potential-flux landscape. We found many interesting quantitative markers for the stability and dynamics: barrier heights between the basins of attraction, MFPT representing the kinetic time of state switching, the EPR representing the thermodynamic cost, and the average flux representing a dynamical driving force for quantifying the global stability of the forest–savanna ecology system. We found that the Flux_{av} and the EPR have the same trends. Their significance changes near (between) the two saddle-node bifurcation points. It is particularly evident for the zero-fluctuation situation with the intrinsic potential landscapes. This demonstrates that the flux and the entropy production rate may provide a dynamical origin and a thermodynamic origin for bifurcation of the nonequilibrium ecological systems, respectively. The dominant paths describing how the state-switching processes actually occur do not follow the naively expected steepest-descent gradient path based on the population-potential landscape alone because of the presence of the nonzero flux. In fact, they are irreversible and determined by both the population-potential landscape and the flux. The flux is the source of the irreversibility.

Remarkably, even though the grassland state is unstable in the deterministic case without fluctuation for certain parameter ranges, it can in fact become quasi-stable under small fluctuations. This may offer a potential explanation for how often treeless grasslands are observed in nature (13, 14), the real existence of which has proved somewhat controversial (53, 54). However, here we show that the emergence of this new stable state under stochastic forcing is predicted by our landscape-flux theory. We therefore suggest a note of caution in the use of empirical frequency distributions to quantify the stability of real landscapes, but also show that, so qualified, empirical frequency distributions can offer useful and rigorous insights into the stability of these biomes.

We provide quantitative and physical markers for identifying the start and end of a bifurcation via the EPR, the Flux_{av}, and the intrinsic free energy. More practically, the information on the physical bifurcation markers, such as the flux and thermodynamics cost of the EPR, can be inferred from the time irreversibility of the observed time traces. Similarly, the variance in the frequency statistics and kinetic time obtained directly from the observed time traces can be used as the kinematic markers for the onset and offset of bifurcations. Therefore, we may be able to identify both physical and kinematic markers to detect the beginning and end of bifurcations in ecological systems based on the observed time series data.

Data Availability. All study data are included in this article and/or *SI Appendix*.

ACKNOWLEDGMENTS. L.X. appreciates support from National Natural Science Foundation of China Grants 11305176 and 21721003, and from the Scientific Instrument Developing Project of the Chinese Academy of Sciences Grant YJKYYQ20180038; J.W. appreciates support from NSF Grant DMS-1951385; S.A.L. and D.P. appreciate support from NSF Grant DMS-1951358; and A.C.S. appreciates support from NSF Grant DMS-1951394.

1. N. G. Van Kampen, *Stochastic Processes in Physics and Chemistry* (Elsevier, Amsterdam, The Netherlands, 2007).
2. V. Volterra, *Lecons sur la Theorie Mathematique de la Lutte pour la Vie* (Gauthier-Villars, Paris, France, 1931).
3. S. E. Jorgensen, G. Bendoricchio, *Fundamentals of Ecological Modelling* (Elsevier, Amsterdam, The Netherlands, 2001).
4. J. Wang, Landscape and flux theory of non-equilibrium dynamical systems with application to biology. *Adv. Phys.* **64**, 1–137 (2015).
5. J. D. Touboul, A. C. Staver, S. A. Levin, On the complex dynamics of savanna landscapes. *Proc. Natl. Acad. Sci. U.S.A.* **115**, 201712356 (2018).
6. A. Staver, S. Archibald, S. Levin, Tree cover in sub-Saharan Africa: Rainfall and fire constrain forest and savanna as alternative stable states. *Ecology* **92**, 1063–1072 (2011).
7. G. Gallopin, Linkages between vulnerability, resilience, and adaptive capacity. *Global Environ. Change* **16**, 293–303 (2006).
8. A. C. Staver, S. Archibald, S. A. Levin, The global extent and determinants of savanna and forest as alternative biome states. *Science* **334**, 230–232 (2011).
9. K. A. Lamothe, K. M. Somers, D. A. Jackson, Linking the ball-and-cup analogy and ordination trajectories to describe ecosystem stability, resistance, and resilience. *Ecosphere* **10**, e02629 (2019).
10. D. Gillespie, Exact stochastic simulation of coupled chemical reactions. *J. Phys. Chem.* **81**, 2340–2361 (1977).
11. R. Thom, *Structural Stability and Morphogenesis* (W. A. Benjamin, 1972).
12. D. Patterson, S. Levin, A. Staver, J. Touboul, Probabilistic foundations of spatial mean-field models in ecology and applications. *SIAM J. Appl. Dyn. Syst.* **19**, 2682–2719 (2020).
13. M. Hirota, M. Holmgren, E. Van Nes, M. Scheffer, Global resilience of tropical forest and savanna to critical transitions. *Science* **334**, 232–235 (2011).
14. V. L. Dantas, M. Hirota, R. S. Oliveira, J. G. Pausas, Disturbance maintains alternative biome states. *Ecol. Lett.* **19**, 12–19 (2015).
15. A. Terebus, C. Liu, J. Liang, Discrete and continuous models of probability flux of switching dynamics: Uncovering stochastic oscillations in a toggle-switch system. *J. Chem. Phys.* **151**, 185104 (2019).
16. A. Terebus, C. Liu, J. Liang, Discrete flux and velocity fields of probability and their global maps in reaction systems. *J. Chem. Phys.* **149**, 185101 (2018).
17. L. Xu, F. Zhang, K. Zhang, E. K. Wang, J. Wang, The potential and flux landscape theory of ecology. *PloS One* **9**, e86746 (2014).
18. A. Staver, Tansley insight: Prediction and scale in savanna ecosystems. *New Phytol.* **219**, 52–57 (2018).
19. M. Scheffer, S. Carpenter, Catastrophic regime shifts in ecosystems: Linking theory to observation. *Trends Ecol. Evol.* **18**, 648–656 (2003).
20. M. Freidlin, A. Wentzell, *Random Perturbations of Dynamical Systems* (Springer, New York, NY, 1984).
21. R. Graham, "Macroscopic potentials, bifurcations and noise in dissipative systems" in *Noise in Nonlinear Dynamical Systems*, F. Moss, P. McClintock, Eds. (Cambridge University Press, 1989), vol. 1, pp. 225–278.
22. G. Hu, *Stochastic Force and Nonlinear Systems* (Science Education Publisher, Shanghai, China, 1995), pp. 225–278.
23. B. Nolting, K. Abbott, Balls, cups, and quasi-potentials: Quantifying stability in stochastic systems. *Ecology* **97**, 850–864 (2016).
24. D. T. Gillespie, The chemical Langevin equation. *J. Chem. Phys.* **113**, 297–306 (2000).
25. P. Ao, Potential in stochastic differential equations: Novel construction. *J. Phys. A* **37**, L25–L30 (2004).
26. P. Zhou, T. Li, Construction of the landscape for multistable systems: Potential landscape, quasi-potential, a-type integral and beyond. *J. Chem. Phys.* **144**, 094109 (2016).
27. L. Wenbo, J. Wang, Uncovering the underlying mechanism of cancer tumorigenesis and development under an immune microenvironment from global quantification of the landscape. *J. R. Soc. Interface* **14**, 20170105 (2017).
28. W. Li, J. Wang, Uncovering the underlying physical mechanism for cancer-immunity of MHC class I diversity. *Biochem. Biophys. Res. Commun.* **504**, 532–537 (2018).
29. E. Dollinger, D. Bergman, P. Zhou, S. X. Atwood, Q. Nie, Divergent resistance mechanisms to immunotherapy explain responses in different skin cancers. *Cancers* **12**, 2946 (2020).
30. P. Zhou, S. Wang, T. Li, Q. Nie, Dissecting transition cells from single-cell transcriptome data through multiscale stochastic dynamics. bioRxiv [Preprint] (2021). https://doi.org/10.1101/2021.03.07.434281 (Accessed 26 May 2021).
31. J. Wang, L. Xu, E. K. Wang, Potential landscape and flux framework of nonequilibrium networks: Robustness, dissipation, and coherence of biochemical oscillations. *Proc. Natl. Acad. Sci. U.S.A.* **105**, 12271–12276 (2008).
32. J. Wang, K. Zhang, L. Xu, E. Wang, Quantifying the Waddington landscape and biological paths for development and differentiation. *Proc. Natl. Acad. Sci. U.S.A.* **108**, 8257–8262 (2011).
33. A. Hastings, Global stability of two species systems. *J. Math. Biol.* **5**, 399–403 (1978).
34. L. Landau, E. Lifshitz, *Statistical Physics Part 1 (Course of Theoretical Physics,*Pergamon Press, Oxford, UK, 1994), vol. 5.
35. J. M. Yeomans, *Statistical Mechanics of Phase Transitions* (Oxford University Press, Oxford, UK, 1992).
36. L. Xu, J. Wang, Curl flux as a dynamical origin of the bifurcations/phase transitions of nonequilibrium systems: Cell fate decision making. *J. Phys. Chem. B* **124**, 2549–2559 (2020).
37. X. Fang, K. Kruse, T. Lu, J. Wang, Nonequilibrium physics in biology. *Rev. Mod. Phys.* **91**, 045004 (2019).

38. E. Schertzer, A. Staver, S. A. Levin, Implications of the spatial dynamics of fire spread for the bistability of savanna and forest. *J. Math. Biol.* **70**, 329–341 (2015).
39. H. Haken, *Advanced Synergetics: Instability Hierarchies of Self-Organizing Systems and Devices* (Springer, Berlin, Germany, 1987).
40. P. Swain, M. Elowitz, E. Siggia, Intrinsic and extrinsic contributions to stochasticity in gene expression. *Proc. Natl. Acad. Sci. U.S.A.* **99**, 12795–12800 (2002).
41. G. Nicolis, I. Prigogine, *Self-Organization in Nonequilibrium Systems: From Dissipative Structures to Order through Fluctuations* (Wiley, New York, NY, 1977).
42. H. Qian, Open-system nonequilibrium steady-state: Statistical thermodynamics, fluctuations and chemical oscillations. *J. Phys. Chem. B* **110**, 15063–15074 (2006).
43. F. Zhang, L. Xu, K. Zhang, E. Wang, J. Wang, The potential and flux landscape theory of evolution. *J. Chem. Phys.* **137**, 065102 (2012).
44. H. Ge, H. Qian, The physical origins of entropy production, free energy dissipation and their mathematical representations. *Phys. Rev. E* **81**, 051133 (2010).
45. H. Yan *et al.*, Nonequilibrium landscape theory of neural networks. *Proc. Natl. Acad. Sci. U.S.A.* **110**, E4185–E4194 (2013).
46. L. Onsager, S. Machlup, Fluctuations and irreversible processes. *Phys. Rev.* **91**, 1505 (1953).
47. M. Freidlin, M. Weber, Random perturbations of dynamical systems and diffusion processes with conservation laws. *Probab. Theor. Relat. Field* **128**, 441–466 (2004).
48. H. Beckett, A. C. Staver, T. Charles-Dominique, W. J. Bond, Pathways of forest savannization in a mesic African savanna-forest mosaic. bioRxiv [Preprint] (2021). https://doi.org/10.1101/2021.05.27.445949 (Accessed 1 June 2021).
49. M. Scheffer *et al.*, Anticipating critical transitions. *Science* **338**, 344–348 (2012).
50. M. Scheffer *et al.*, Early-warning signals for critical transitions. *Nature* **461**, 53–59 (2009).
51. H. Qian, E. Elson, Fluorescence correlation spectroscopy with high-order and dual-color correlation to probe nonequilibrium steady state. *Proc. Natl. Acad. Sci. U.S.A.* **101**, 2828–2833 (2004).
52. K. Zhang, J. Wang, Exploring the underlying mechanisms of the Xenopus laevis embryonic cell cycle. *J. Phys. Chem. B* **122**, 5487–5499 (2018).
53. N. P. Hanan, A. T. Tredennick, L. Prihodko, G. Bucini, J. Dohn, Analysis of stable states in global savannas: Is the cart pulling the horse? *Global Ecol. Biogeogr.* **23**, 259–263 (2014).
54. A. C. Staver, M. C. Hansen, Analysis of stable states in global savannas: Is the cart pulling the horse? -a comment. *Global Ecol. Biogeogr.* **24**, 985–987 (2015).